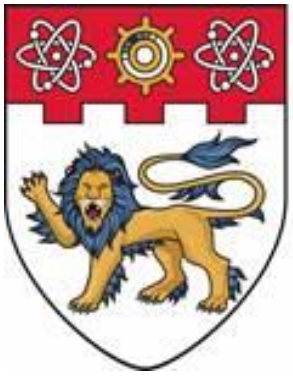

NANYANG TECHNOLOGICAL UNIVERSITY
SINGAPORE

FINAL YEAR PROJECT REPORT

SCSE23-1085: DEVELOPMENT OF APPLICATION FOR PATTERN PROJECTION AND COMPARATIVE ANALYSIS OF BINARY DEFOCUSING TECHNIQUES IN FRINGE PROJECTION PROFILOMETRY

Submitted by : Hendy

Matriculation Number: U2122559J

Project Supervisor: Assoc. Prof Qiao Kemao

Examiner: Assoc. Prof Alexei Sourin

Academic Year 2023/2024

College of Computing and Data Science

A final year project report presented to Nanyang Technological University
in partial fulfilment of the requirements for the degree of Bachelor of Computer Science

2024

Abstract

Fringe Projection Profilometry (FPP) is a highly accurate non-contact 3D measurement technique that uses a DLP projector to generate and project structured patterns onto an object's surface to capture its surface information. However, the DLP projector used in FPP has a limitation of speed bottleneck typically around 247 Hz which presents a significant challenge in dynamic measurement applications [4].

This project aimed to address this speed bottleneck issue using binary defocusing techniques and developing software to control the projection. The enhancements were designed to improve projection speed, enabling faster and more efficient 3D surface reconstruction without compromising accuracy. Experimental results demonstrated that the optimized FPP system can effectively handle high-speed measurements, expanding its applicability in real-time industrial and research environments.

Acknowledgements

I would like to express my gratitude to following people for their guidance and support towards the accomplishment of this final year project.

Associate Professor Qiao Kemao. Who is my supervisor, he shared his opinions and provided feedbacks on the project.

Lyu Shenzhen and **Huang Nengqi** for guiding me through the project and providing me with the necessary information to close the knowledge gaps required for this project scopes.

Table of Contents

List of Figures

List of Equations

Chapter 1

Introduction

1.1 Background

3D measurement techniques have become indispensable in fields such as manufacturing, healthcare, and research, enabling the accurate capture of real-world objects' geometric and surface details. These techniques offer various methods for collecting three-dimensional data, each with its own strengths and trade-offs depending on the specific application. The growth and advancement of modern information technology have significantly promoted the adoption of 3D measurement across various fields, providing benefits such as the creation of precise digital 3D CAD models in industrial design, the use of 3D sensing technology in intelligent manufacturing, and the ability to perceive and interpret the 3D environment for automation and robotics [1].

FPP also plays an important role in a variety of applications, including biological imaging and manufacturing quality control. Its application in dynamic circumstances, such as tracking the movement of objects in real-time or monitoring the deformation of materials under stress, is further enhanced by its ability to capture exact surface geometry quickly. The importance of FPP in expanding technical applications across a range of industries is highlighted by its versatility and capacity to achieve measurement precision.

There are many different methods to measure the 3D shape of an object, among the most prominent 3D measurement techniques are contact-based methods, laser scanning, stereo vision, and Fringe Projection Profilometry (FPP).

Fringe Projection Profilometry (FPP) is a 3D optical measurement technique widely used due to its low cost, high speed, and high accuracy in capturing the 3D shape of an object. FPP works by using a projector to project a series of fringe patterns onto the surface of the target 3D object and using the camera to capture and analyze the deformation of these patterns to extract the depth information of the 3D object.

This project explored the FPP technique for its non-contact and accurate measurement features. FPP is useful for measuring complicated or fragile surfaces without causing harm. High-resolution 3D measurements can be made with FPP while limiting interference with the target

object. FPP is a special type of structure light projection technique that is used for 3D measurements. There are other structured lights like speckle patterns, and FPP uses fringe patterns., leveraging structured light patterns to extract precise surface geometry of objects. This method is especially advantageous due to its ability to capture high-resolution data across complex surfaces, making it suitable for applications ranging from industrial inspection to medical imaging and reverse engineering.

Zhang et al. (2022) described in [2] that general FPP measurement stages involved:

1. **Pattern Projection**, projecting a sequence of structural fringe patterns onto the object using a projector.
2. **Image Acquisition,** using a camera to record the fringe patterns that are projected onto the object's surface. The surface geometry causes the patterns to deform, and these distorted patterns are captured as images by the camera.
3. **Phase Measurement**, converting inverse trigonometric functions into phase values allows one to assess the height profile and correspondence between the camera and projector.
4. **Phase Unwrapping,** obtaining a continuous phase map of the captured target.
5. **3D reconstruction**, taking the processed phase data and using it to create a continuous 3D form of the object.

There are also additional steps such as **Camera Calibration** involve tuning the intrinsic (focal length) and extrinsic parameters (position of the camera and the orientation of the 3D object). This is essential to achieve triangulation, which allows the system to derive depth information from the projected patterns. The system was able to determine the 3D coordinates of points on the object's surface by calculating the angles and separations between the projector, camera, and object.

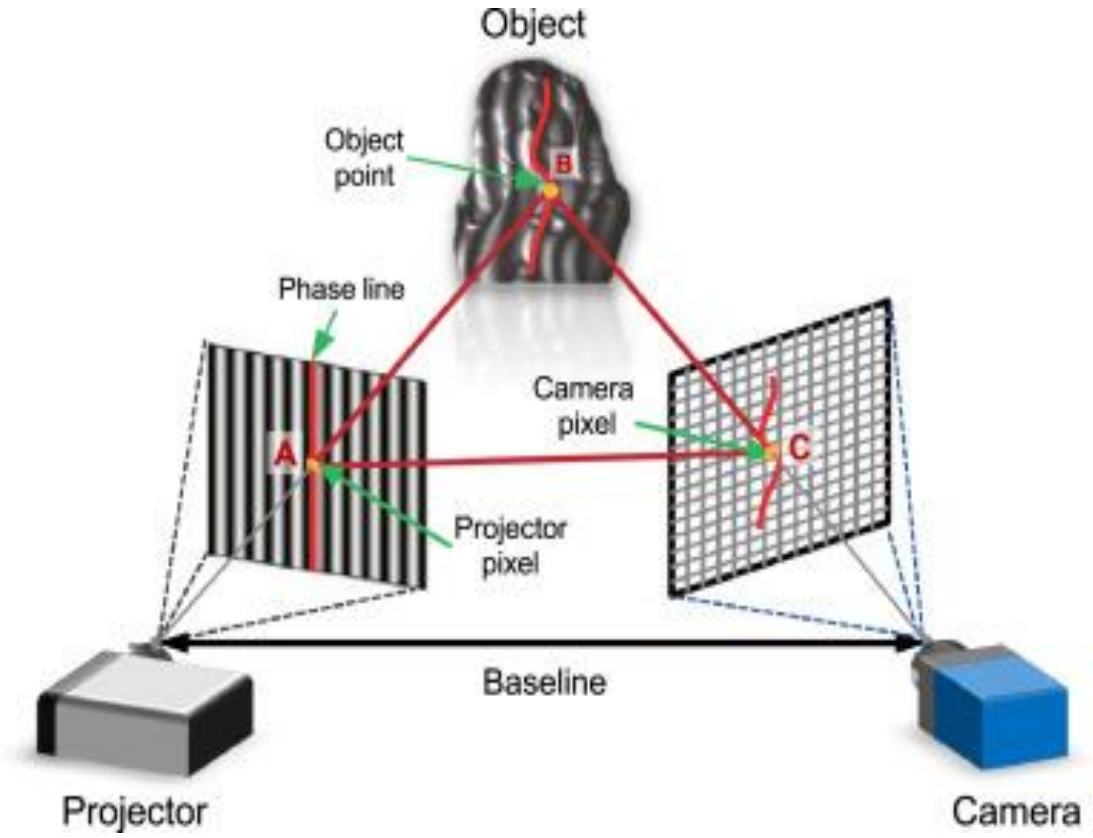

Figure 1.1 Performing 3D measurements with fringe projection profilometry [3].

1.2 Motivation

With the help of the DLP projector, FPP techniques can achieve high-accuracy 3D measurement. However, there was a limitation in using the technology to achieve high measurement speed, The DLP projector has a limitation of the speed bottleneck at 247 Hz which came from the 8-bit representation of an ideal sinusoidal pattern [4].

Lei and Zhang (2009) [5] have proposed the use of binary-defocusing techniques to solve this problem. By Utilizing 1-bit binary patterns with lens defocusing effect from the projector, high accuracy can be achieved while greatly increasing measurement speed. The reason for using 1-bit binary patterns is because the maximum speed for the 1-bit pattern is around 1000 Hz [4].

Binary defocusing techniques enhanced the accuracy and speed by suppressing the higher-order harmonics of the square wave in Fourier series expansion. This could be achieved through

projector defocusing suppressing the higher order harmonics of a square wave resulting in first-order harmonic (sinusoidal) to be dominant in the resultant pattern [6].

Past researchers have done experiments using dithering techniques such as Bayer matrix dithering [7], error diffusion dithering [8], and Phase-optimized dithering [9] has shown prominent success in binary defocusing techniques. The result of the dithering techniques will then be defocused by the projector before it is projected to the target object.

This project focuses on addressing the speed limitations of FPP techniques by implementing binary defocusing approaches and comparing various dithering methods. The goal is to enhance the speed and accuracy of FPP, making it more suitable for real-time applications. The findings aim to contribute to the field by providing a pathway toward overcoming the current speed constraints in 3D measurement technology.

1.3 Project Scope

The project focused on the improvement made on the pattern projection and image acquisition stages of FPP with the use of the DLP LightCrafter 6500 projector. Digital Light Processing (DLP) projector is a display technology developed by Texas Instruments and widely used for projecting high-resolution patterns in applications related to 3D objects. The project aimed to compare and integrate advanced techniques for improving the speed and accuracy of FPP measurements through the implementation of binary defocusing techniques. The project also involved software development using Qt for projecting fringe patterns, which included functions that help to achieve fine-tuned control over binary defocusing processes and pattern generation.

1.4 Objective

The objective of this project was to advance FPP techniques through the implementation of binary defocusing techniques to allow 8-bit images to achieve the speed of 1-bit images (1000 Hz). This project further aimed to develop software that can be used to project the fringe

patterns, a custom standalone software enabled the user to include features to fine-tune control over the binary defocusing technique process and pattern generation process. This project hopes to achieve a faster, more precise, and more dependable 3D reconstruction process through the improvement of pattern projection. Furthermore, experiments have been conducted to compare the performance of different methods of dithering that were significant to binary defocusing techniques.

1.5 Contribution

The significance of this project lies in its potential to enhance the performance of FPP technology, making it more suitable for real-time measurement applications and scenarios involving dynamic objects. Accelerated 3D modeling capabilities would benefit numerous industries, such as additive manufacturing, where rapid scanning is essential for layer-by-layer model construction, and the medical field, where accurate and timely measurements are critical for patient care. This project also developed a standalone application using Qt, enabling pattern editing and direct updates to the DLP projector, paving the way for adding custom functions required by users. Future work could involve enabling communication between the application, the camera, and the projector, further automating the measurement process.

Chapter 2

Literature Review

This section explored past research and experiments conducted by various researchers in the field of Fringe Projection Profilometry (FPP).

Wang and Zhang (2012) introduced the concept of using Bayer dithering (halftoning) and defocusing to optimize binary patterns into high-quality fringe patterns. They utilized the Bayer-ordered dithering technique due to its strong performance and ease of operation. Their research involved five-phase shifting to generate two different sets of binary dithered patterns with periods T1 = 600 pixels and T2 = 150 pixels. They compared the relative root mean square (RMS) errors of the fringe patterns after defocusing, concluding that the pattern with T2 = 150 pixels achieved a lower error rate, indicating better accuracy in reproducing fringe patterns compared to the longer-period pattern. Additionally, they compared the 3D results from the dithered patterns with those from ideal sinusoidal patterns, demonstrating that the dithered patterns yielded closer approximations to the actual surface geometries. Their findings emphasized the importance of selecting appropriate dithered patterns to enhance the fidelity of fringe projection and the overall accuracy of 3D shape measurements [7].

In a subsequent study in 2013, Lohry and Zhang advanced the optimization of dithering techniques by employing an error diffusion algorithm to refine binary dithering for sinusoidal structured fringe pattern generation. They claimed that the genetic method using error diffusion dithering techniques is more accurate because it distributes quantization error to neighboring pixels, resulting in smoother gradients perceived by the human eye. This process minimizes abrupt transitions between intensity levels, reducing artifacts in the projected fringe patterns. Their experiments highlighted that using error diffusion significantly improved image quality, particularly in complex surface measurements. Moreover, they conducted a series of tests to evaluate the impact of dithering techniques on different material surfaces and lighting conditions, concluding that the error diffusion method outperformed traditional dithering techniques in terms of 3D reconstruction accuracy [8].

Dai et al. (2013) took further steps to enhance fringe quality through a phase-optimized dithering technique. Their research demonstrated that optimizing the dithering pattern to match

the phase characteristics of the projected fringe patterns could yield higher-quality 3D shape measurements. They also explored the mathematical formulations behind phase optimization, showing that precise control over the fringe pattern significantly reduced measurement errors associated with phase wrapping and unwrapping. This method aimed to reduce errors in the phase map by improving the consistency of the fringe patterns during projection and acquisition, which is essential for accurate surface reconstruction in FPP applications. Their findings indicated significant improvements in reducing phase errors compared to standard dithering techniques, making phase-optimized dithering a valuable approach for applications requiring high precision. Additionally, they provided detailed performance metrics, illustrating the trade-offs between different dithering strategies in various experimental setups [9].

In this project, incorporating various dithering techniques such as Bayer matrix dithering, error diffusion, and phase-optimized dithering was considered to enhance the performance of binary defocusing in Fringe Projection Profilometry (FPP). The previous research by Wang and Zhang (2012) demonstrated that Bayer dithering could effectively optimize fringe patterns, achieving lower RMS errors for shorter fringe periods, which indicates better pattern quality. Lohry and Zhang (2013) further highlighted the advantages of error diffusion, which distributes quantization error to neighboring pixels, thus improving the smoothness of projected patterns and reducing artifacts. Additionally, Dai et al. (2013) showed that phase-optimized dithering could significantly reduce phase errors by matching the phase characteristics of fringe patterns, improving the accuracy of 3D measurements. By applying these dithering techniques, this project aims to leverage their unique strengths to achieve a balance between measurement speed and quality in FPP, particularly when using a DLP projector for pattern projection. Each technique provides different benefits that can be tailored to the measurement requirements and surface characteristics, potentially enhancing the accuracy and efficiency of the 3D reconstruction process.

Li et al. (2013) introduced two distinct approaches for improving 3D measurement quality through binary defocusing techniques. The first approach involved the use of sinusoidal pulse width modulation (SPWM), where the unwanted higher-order harmonics are shifted to higher frequencies. This shift makes the harmonics less significant within the projected fringe patterns, allowing for a small degree of defocusing to be effective in smoothing out the pattern and reducing errors. However, it was found that SPWM performs better than the standard square binary method only within a specific range of fringe periods [11].

These techniques are highly relevant to the use of DLP projectors in Fringe Projection Profilometry (FPP). The DLP projector’s inherent capability for high-speed modulation makes it well-suited for implementing SPWM, as it can rapidly switch the mirror positions to achieve the required modulation of light intensity. However, SPWM requires careful calibration of the projector's defocusing level and pattern frequency to achieve optimal results. Thus, while SPWM can enhance measurement quality by shifting undesired harmonics away from the dominant frequencies, its effectiveness is limited to cases where the fringe period is suitably chosen.

Chapter 3

Working Mechanisms of Fringe Projection Profilometry (FPP)

The Fringe Projection Profilometry (FPP) process starts with camera calibration, this step involves measuring intrinsic parameters, such as focal length and lens distortion, this step also measures the extrinsic parameters, such as the spatial positions and orientations of the camera, projector, and target object. These measurements are recorded to ensure accurate triangulation (utilizing the positions of the camera and projector to derive precise 3D coordinates) and correspondence (ensuring that data points from the captured images accurately reflect the target object's surface characteristics). This calibration step is crucial for minimizing measurement errors and ensuring smooth communication between the camera and the projector during the object capture process. It also enables the system to account for various optical and geometric distortions that may affect the quality of the reconstructed 3D model, ultimately enhancing the accuracy and reliability of the entire FPP system.

After camera calibration, Zhang et al. (2022) specified other important steps including the next step, **Pattern Projection** which involves the projector projecting the predefined patterns onto the object and the distortion of the pattern on the target object will then be recorded using a camera in the **Image Acquisition** phase to achieve correspondence between the camera and projector. **Phase Measurement** will then be calculated to obtained phase range from $-\pi$ to π.

Phase is used as a measurement variable because phase directly correlates to the target object's height based on the wavelength projected by the projector. To further reduce noises such as fluctuating light intensity, sensor sensitivity, or external environmental factors, **Three-phase shifting algorithm** is also implemented into FPP. It involves projecting three different fringe patterns that are shifted in phase from one another to enhance the data acquisition process by providing more phase information, this helps resolve ambiguities in the captured images. When the phase of the projected patterns is varied in this systematic manner, it allows the reconstruction algorithm to accurately discern the height variations of the object's surface. The additional phase information helps in reducing measurement errors and improves the robustness of the height profile extraction, especially in challenging scenarios where the surface is complex, or the lighting conditions are variable [3].

Three-phase shifting algorithms can be implemented and calculated into three different shifted light intensities shown in Equation 1 [10].

$$I_1(x,y) = I'(x,y) + I''(x,y)\cos[\varphi(x,y) - 2\pi/3],$$

$$I_2(x,y) = I'(x,y) + I''(x,y)\cos[\varphi(x,y)],$$

$$I_3(x,y) = I'(x,y) + I''(x,y)\cos[\varphi(x,y) + 2\pi/3]. \quad (1)$$

I1, I2, and I3 denote the intensities of different phases.

Its wrapped phase can then be calculated with Equation 2

$$\phi(x,y) = \tan^{-1}\left[\frac{\sqrt{3}(I_1 - I_3)}{2I_2 - I_1 - I_3}\right] \quad (2)$$

Which ranges from -π to π. And need to be unwrapped.

After the three-phase shifted fringe patterns were shined on the target object, the camera captured the deformed fringe patterns projected on the target object's surface. The surface distortion caused by surface geometry and its texture will be recorded by the camera. After capturing the deformed fringe patterns, the next step involves **Phase Unwrapping**, which is essential for converting the wrapped phase values (which range from $-\pi$ to π) into continuous phase values. This process is critical for accurately reconstructing the 3D shape of the object since wrapped phases can lead to ambiguities in the height measurements.

Once the phase information is unwrapped, **3D reconstruction** is performed by taking the processed phase data and using it to create a continuous 3D form and build it into a 3D model using triangulation. The relationship between the projector, camera, and the object's surface allows for the calculation of the 3D coordinates of points on the object by utilizing the known positions of the camera and projector along with the measured phase data. Triangulation effectively derives the depth information from the captured images by analysing the angles formed between the projector's projection and the camera's view of the object.

Chapter 4

Methodology

This section outlines the procedures and techniques employed in the study to achieve the desired outcomes in fringe projection and 3D reconstruction. The methodology encompasses several key processes, including the generation of ideal sinusoidal patterns, the application of dithering techniques, and the assessment of their impact on image quality.

In this project, some of the parameters were set, such as period = 36 pixels, exposure time = 20000 microseconds, and dark time = 5000 microseconds.

4.1 Generate Ideal Sinusoidal Patterns

To establish a benchmark for evaluating the quality of fringe projection and 3D reconstruction, an ideal sinusoidal pattern was computed using a mathematical function that simulates a continuous sinusoidal wave. This ideal pattern served as a reference for comparison with patterns generated using various dithering and defocusing techniques.

An ideal sinusoidal pattern is expressed as:

$$I(x,y) = \frac{I_{\max} + I_{\min}}{2} + \frac{I_{\max} - I_{\min}}{2} \cos\left(\frac{2\pi}{T}x + \phi\right) \quad (3)$$

$I_{(x,y)}$ represent the pixel intensity.

I_{max} and I_{min} are the maximum and minimum intensity values.

T is the fringe period.

ϕ is the phase shift.

Equation 3 generated smooth sinusoidal intensity variations, which were crucial for achieving accurate 3D shape measurements.

An ideal sinusoidal pattern was computed through

```
% Parameters
width = 1920;
height = 1080;
bitdepth = 8;
period = 36;

% Create mesh grid for image dimensions
[X, Y] = meshgrid(1:width, 1:height);

% Generate phase shift values
phase = 2 * pi / period * X;

% Generate sinusoidal patterns with three phase shifts
I1 = 0.5 + 0.5 * cos(phase - 2 * pi / 3);
I2 = 0.5 + 0.5 * cos(phase);
I3 = 0.5 + 0.5 * cos(phase + 2 * pi / 3);

% Calculate the wrapped phase
phaseOgri = atan2(sqrt(3) * (I1 - I3), 2 * I2 - I1 - I3);

% Plot the sinusoidal patterns
figure;
imshow(phaseOgri, []);
title('Wrapped Phase \phi_{Original}');
```

Figure 4.1a MATLAB codes for generating ideal sinusoidal pattern

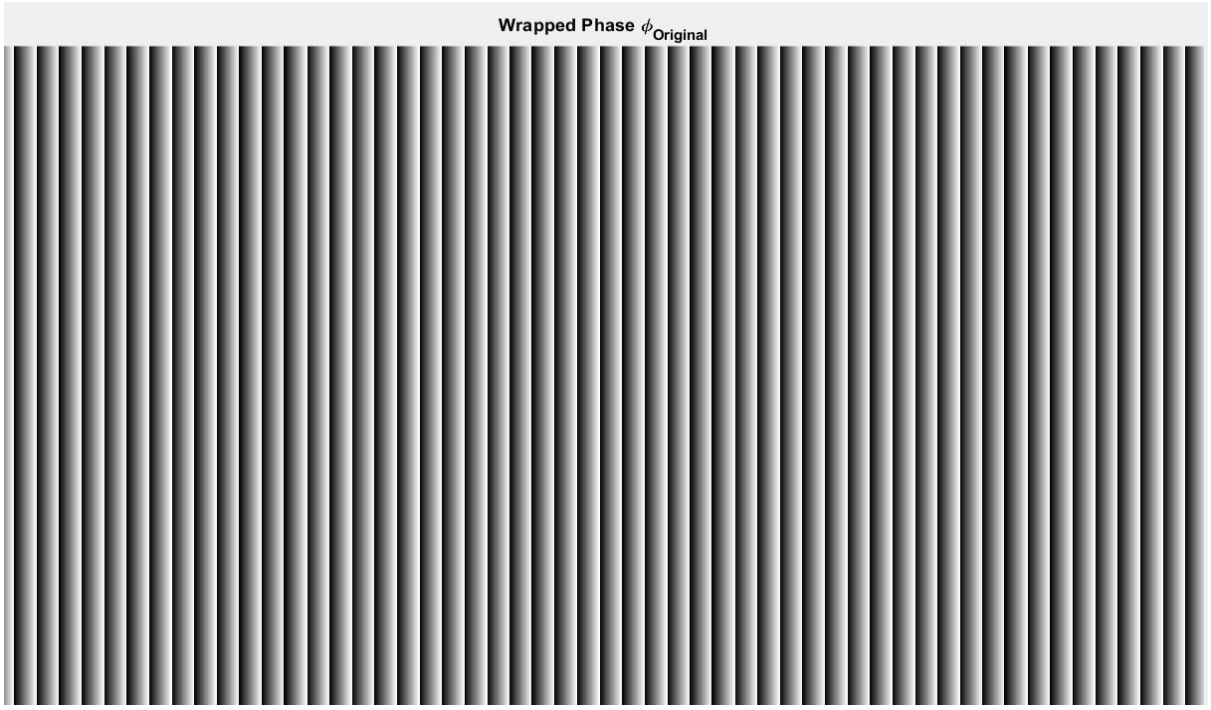

Figure 4.1b 8-bit ideal sinusoidal pattern at T = 36

The purpose of generating ideal sinusoidal patterns was for comparison of :

1. **Benchmarking quality**, the ideal sinusoidal pattern generated can provide a reference to evaluate how closely the projected binary patterns (generated through dithering techniques) replicate the smoothness and continuity of a true sinusoidal wave. By comparing the binary dithered patterns to the ideal pattern, the phase errors and distortions were calculated and compared.

2. **Phase Accuracy Evaluation**, a three-phase shifting algorithm used three phase shifted versions of the sinusoidal pattern (with intensities I1, I2, and I3) to compute the wrapped phase. I1 shifted $2\pi/3$ to the left and I3 shifted $2\pi/3$ to the right. This computed phase is denoted as **"phaseOgri"** (shown in Figure 4.1a) and serves as the ground truth for phase comparison. The accuracy of the binary defocused was measured against this reference phase to identify deviations and the root mean square (RMS) error was calculated.

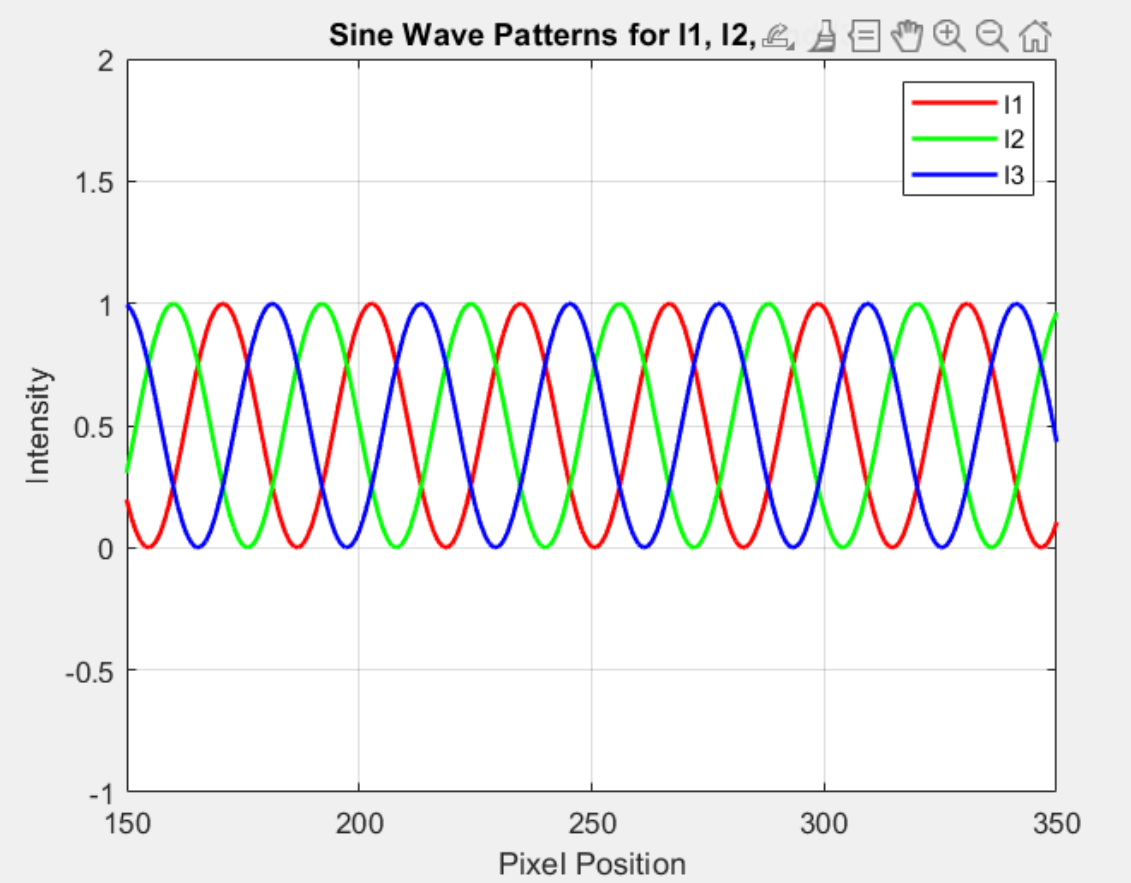

Figure 4.2. sines wave after applying three-phase shifting at T=36

3. **Validation of Defocusing Techniques**: Since binary patterns inherently introduce quantization artifacts and discontinuities, projector defocusing was employed to blur the projected patterns and mimic the appearance of a continuous sinusoidal pattern. Comparing the results after applying binary defocusing to the ideal sinusoidal pattern allowed assessment of how effectively defocusing reduces artifacts and improves phase reconstruction.

4. **Error Analysis and Optimization**: By quantifying the phase differences between the ideal sinusoidal pattern and the dithered/defocused patterns, the performance of different dithering techniques can be objectively evaluated. This analysis is crucial for selecting or optimizing dithering methods to achieve the highest possible accuracy in 3D surface reconstruction.

Next, the binary defocusing technique was implemented by applying binary dithering techniques on each of the I1, I2, and I3.

4.2 Apply Binary dithering Techniques

This section discussed various binary dithering methods used to convert grayscale patterns into binary patterns. The objective of dithering is to approximate the continuous grayscale levels by adjusting the arrangement of black and white pixels. Different dithering methods have unique characteristics in how they balance image quality, computational complexity, and adaptability to different patterns.

The binary dithering techniques were applied to the I1, I2, and I3 images obtained from the ideal sinusoidal patterns. The results were then compared with the ideal phase values derived from the reference patterns. To quantify the difference between the dithered and ideal phase values, there was a need to use a suitable metric. The Root Mean Square (RMS) error was chosen for this purpose because it effectively measures the magnitude of deviations by calculating the square root of the average squared differences between the dithered and ideal phase values. RMS error was particularly suitable for this analysis as it provides a clear indication of the overall accuracy by emphasizing larger errors, thus helping to evaluate the quality and fidelity of the reconstructed 3D shapes in Fringe Projection Profilometry (FPP).

$$\text{RMS Phase Error} = \sqrt{\frac{1}{N}\sum_{i=1}^{N}(\phi_{\text{measured},i} - \phi_{\text{ideal},i})^2}$$

Where:

- $\phi_{\text{measured},i}$ is the measured phase at point i
- $\phi_{\text{ideal},i}$ is the ideal phase at point i

(4)

RMS value is commonly used to measure the magnitude of variation, and it is calculated by taking the square root of the mean of the squares of the values. RMS provided sensitive measurement of the deviations between the actual and expected values.

RMS value converted the phase differences into a single scalar quantity, facilitating direct comparison across different configurations or measurement techniques. This was particularly important in applications such as fringe projection profilometry, where variations in phase due to environmental conditions or system calibration can significantly impact measurement accuracy.

4.1.1 Bayer Ordered Dithering Technique

Bayer Ordered Dithering works by comparing each block of the original image pixels to a threshold kernel in the form of a Bayer matrix.

Bayer matrix is usually the size of 2^N (N is an integer) and its base form (smallest) is in the form of a 2x2 matrix shown below.

$$M_1 = \begin{bmatrix} 0 & 2 \\ 3 & 1 \end{bmatrix}$$

A larger grid for the Bayer matrix can be obtained by performing calculations shown in Equation 5.

$$M_{n+1} = \begin{bmatrix} 4M_n & 4M_n + 2U_n \\ 4M_n + 3U_n & 4M_n + U_n \end{bmatrix} \quad (5)$$

Where U_n is a n x n unit matrix [6].

Bayer Ordered Dithering works by the following steps:

1. **Matrix setup**, assigning a Bayer matrix size of m x m to be constructed.
2. **Intensity comparison and mapping,** the Bayer matrix constructed was used to compare with the original image pixel by pixel. the values in the Bayer matrix were treated as thresholds and if the original image pixel value was bigger than threshold, the pixel was be assigned a value of "1" otherwise, it was assigned a value of "0".

The output was a binary image after comparing all the pixels of the original image maintained overall brightness levels and some visual appearance of the original image can still be visible, though the image appeared to be rendered.

Increasing the grid of the Bayer matrix encouraged smoother gradients and reduced visible banging. A larger Bayer matrix size also meant that the quantization error could be spread to become more effective across a bigger area of the image. However, it also increased the computation load and memory usage.

Bayer ordered dither was beneficial because it required less computational resources, and it was suitable for real-time applications. It was especially useful to be applied to grayscale images, making it versatile in both imaging and display technologies. However, the Bayer matrix fixed threshold value may not be well adapted to all types of images, and it is not suitable to be used if the original image is already a 1-bit image.

4.1.2 Error Diffusion Dithering Technique

Error Diffusion dithering works by distributing the quantization errors from the original grayscale pixel value to its neighboring pixels. This method ensures that the intensity levels in the resulting binary image more closely resemble the original image's gradients and details.

The process of modifying an input pixel can be described in Equation 6 [8].

$$\tilde{f}(i,j) = f(i,j) + \sum_{k,l \in S} h(k,l)e(i-k, j-l). \quad (6)$$

The quantization error was distributed in the proportion shown below where X is the pixel to transfer the quantization error from:

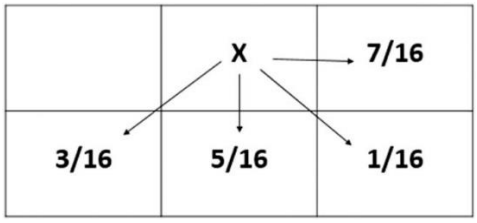

And it can be interpreted as Floyd-Steinberg Kernel:

$$\frac{1}{16}\begin{bmatrix} - & * & 7 \\ 3 & 5 & 1 \end{bmatrix}.$$

Where " – " represents the previously processed pixels and " * " represents the current computing pixel.

Figure 4.3 refers to the code showing how the error diffusion dithering works.

```
errordifmatrix = [0 0 7; 3 5 1] / 16;

function ditheredImage = errorDiffusionDitherSingle(image, errordifmatrix, height, width)

    ditheredImage = zeros(height, width);

    % Process the image pixel by pixel
    for i = 1:height-1
        for j = 2:width-1

            % Quantize this pixel
            oldPixel = image(i, j);
            newPixel = round(oldPixel);
            error = oldPixel - newPixel;

            % Assign to current pixel [i,j]
            ditheredImage(i, j) = newPixel;

            % Diffuse the error to neighboring pixels
            image(i, j+1)   = image(i, j+1)   + error * errordifmatrix(1,3);  % 7/16
            image(i+1, j-1) = image(i+1, j-1) + error * errordifmatrix(2,1);  % 3/16
            image(i+1, j)   = image(i+1, j)   + error * errordifmatrix(2,2);  % 5/16
            image(i+1, j+1) = image(i+1, j+1) + error * errordifmatrix(2,3);  % 1/16
        end
    end
end
```

Figure 4.3. MATLAB codes for generating error diffusion dither patterns.

Error diffusion dither worked by the following steps:

1. **Error calculation for the pixel**, calculated the difference between the original image pixel and its round value.
2. **Error distribution**, the calculated error was then distributed to its neighboring pixel based on the Floyd-Steinberg Kernel weight.

The steps were repeated until all the pixels in the original image were processed.

The advantages of using the error diffusion dithering mentioned in [7] were to improve Image quality as the method reduced visible banging and created soother gradients. Error diffusion dithering also enabled dynamic adjustment that can be adopted to various image types.

The disadvantage of error diffusion dithering includes increased computational load compared to ordered Bayer ordered dithering.

4.1.3 Optimized Phase Dithering Technique

Optimized Phase dithering aimed to enhance the quality of the fringe patterns in 3D shape measurement applications. This method helped reduce phase errors and improved the accuracy of surface reconstruction by optimizing the dithering patterns used during the projection process.

Optimized Phase Dithering works by the following steps [9]:

1. Error pixel detection, pattern after dithered with Bayer Dithering the phase error is then calculated with Equation 7

$$\Delta_{\Phi}(i,j) = \left| \Phi(x,y)^{i} - \Phi^{d}(x,y) \right| > \epsilon \quad (7)$$

   And marked it as the error pixel where E is denoted as the threshold value (0.1 rad)
2. Error pixel mutation, each pixel will be inverted (0 to 1 and 1 to 0) and the difference of the phase map was computed again and if there is a reduction of the error, the inverted value was kept, and the RMS error was updated, otherwise revert the inverted pixel back.

This process was repeated till all the pixels had been processed. And it repeated the process again for a few iterations while reducing the threshold amount. **A converges threshold of 0.01** and max iterations were set to stop either after certain iterations or after the algorithm converges.

The advantages of the optimized phase dithering technique were that the pattern generated will have a better surface reconstruction as the error keeps reducing. However, the effectiveness of phase-optimized dithering may be highly dependent on the specific characteristics of the projected fringe patterns, potentially limiting its versatility across different applications.

The Figure 4.4 shows the comparison between ideal sinusoidal patterns and its binary dithered pattern.

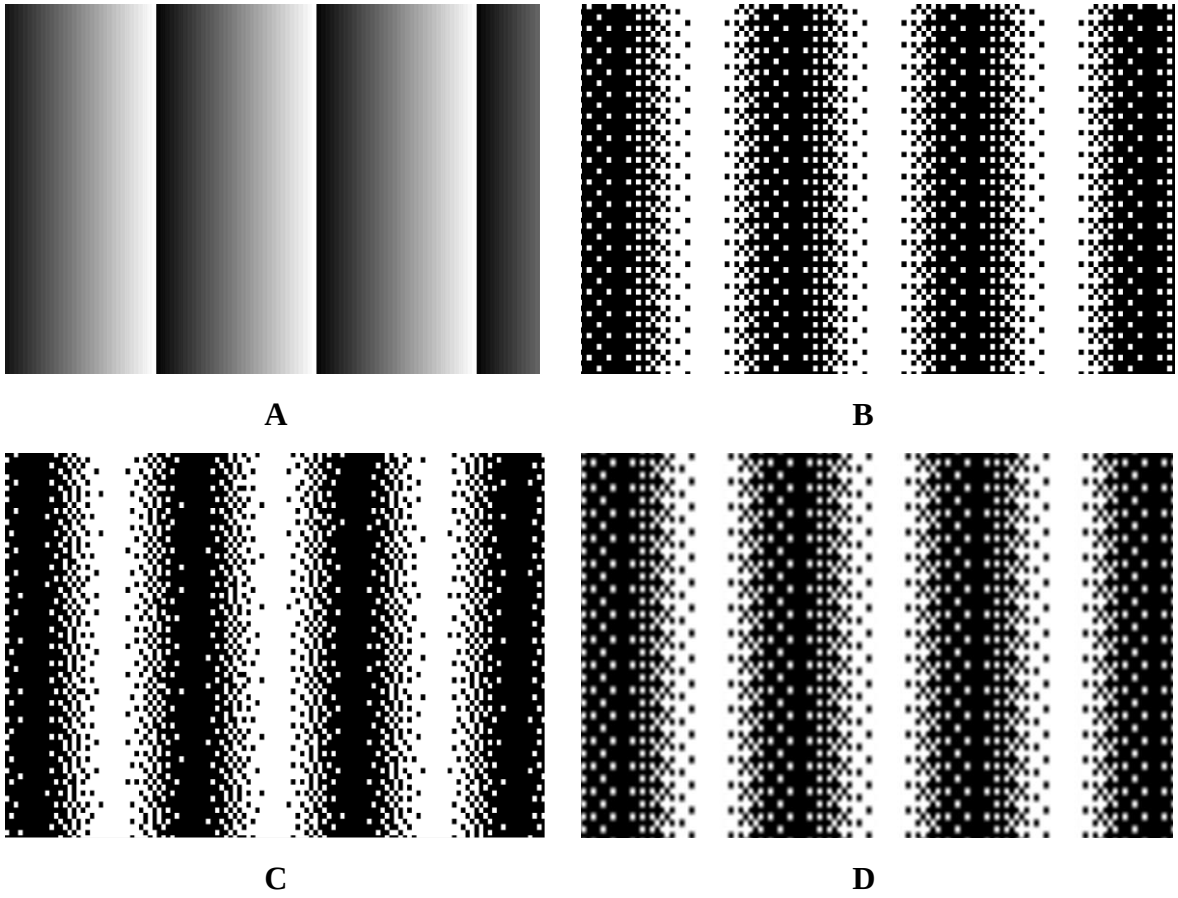

*Figure 4.4. Different pattern representation **(A)** 8-bit fringe pattern, **(B)** Result after Bayer ordered dithering of A, **(C)** Result after error diffusion dithering of A, and **(D)** Result after optimized phase dithering of A.*

4.3 Apply Patterns Defocusing

To further enhance the quality of binary patterns and ensure the project patterns closely mimic the smoothness of ideal sinusoidal patterns, **defocusing techniques** were applied to the projected binary patterns. This was critical for reducing quantization artifacts introduced by binary dithering and for achieving higher accuracy in the phase measurement of the 3D surface reconstruction.

The steps for applying pattern defocusing in this project were outlined as follows:

1. **Evaluate Binary dithering result with Gaussian filter**:
    - To achieve the best result, the first step was to determine the best Gaussian filter size to be assigned. Root means square error was calculated and several different Gaussian filter sizes were tested [1, 3, 5, 7, 11, 13] with all the different binary dithering techniques to determine the best filter size to be used in this project.
2. **Setup for Defocusing**:
    - The projector's focus was changed to complete the defocusing procedure. To prevent excessive blurring, which could skew the projected pattern and reduce overall accuracy, the amount of defocusing was carefully adjusted.
    - The goal was to identify the optimal defocus level where the projected binary patterns approximated the smoothness of the ideal sinusoidal patterns without losing critical phase information.
3. **Application of Defocusing to Dithered Patterns**:
    - The binary patterns generated through **Bayer Ordered Dithering**, **Error Diffusion Dithering**, and **Optimized Phase Dithering** were projected sequentially onto the target surface.
    - The projector’s optics were then slightly defocused during the projection of each pattern. By adjusting the focus, the sharp edges of the binary patterns were softened, effectively creating a blurred version of the original pattern.

- The defocused patterns were captured by the camera, and the deformed fringes on the surface of the object were analyzed to assess how well the defocusing technique improved phase accuracy.

4. **Evaluation of Defocused Patterns**:
    - After applying defocusing, the captured fringe patterns were processed to extract the wrapped phase information. This phase was compared to the phase obtained from the ideal sinusoidal patterns to determine the effectiveness of the defocusing process.
    - Key metrics such as root mean square (RMS) error, phase distortion, and artifact reduction were used to quantify the improvements brought by defocusing.
    - It was observed that **slight defocusing** significantly reduced phase errors by blurring the high-frequency components caused by dithering, resulting in smoother and more continuous phase maps. However, **excessive defocusing** led to loss of detail and degradation in surface reconstruction accuracy.
5. **Optimization of Defocusing Parameters**:
    - Based on the results of the evaluation, the defocus level was fine-tuned to achieve the optimal balance between reducing quantization artifacts and preserving the integrity of the projected patterns.
    - Further iterations involved adjusting the projector's focal distance and performing multiple tests to ensure that the defocusing technique was effective across various dithering methods and target surfaces.

By applying the defocusing technique to the binary dithered patterns, significant improvements in phase accuracy were achieved, allowing the 3D surface reconstruction process to yield more reliable results. This technique serves as a crucial step in overcoming the limitations of binary patterns and enhancing the overall precision of FPP.

4.4 Developing Software using QT

This section explored the software developed using QT. The motivation for using Qt in this project stems from its robust features and versatility in developing cross-platform applications. Qt provides a comprehensive set of tools for creating intuitive and responsive user interfaces, essential for managing the complexities associated with controlling the projector. Its signal-slot mechanism simplifies the handling of events, which is particularly beneficial for real-time applications like fringe projection.

4.4.1 About QT

Figure 4.5 Qt for Python

Qt is a popular tool used for developing applications. Qt is open-source and easy to use. Qt supports programming in Python language with the only requirement being to have at least Python version 3.8. This project aimed to project the patterns set and possibly provide the flexibility of creating custom functionality to communicate with the camera and projector for better correspondence.

For this project, Qt for Python (using the PySide6 library) was employed to integrate the Qt6 API functionalities into Python-based applications. PySide6 allowed access to a wide range of Qt tools and functions, making it suitable for creating graphical user interfaces and managing hardware interaction. Utilizing Qt for Python offered a smooth development experience by combining the simplicity of Python with the powerful features of Qt [12].

PySide6 allowed python to access Qt tools and functions for both desktop and embedded systems, which was beneficial for controlling devices like the DLP LightCrafter.

Features of Qt that are relevant to DLP LightCrafter Development:

- Cross-Platform Compatibility: Qt enables programmers to create code only once and have it run on a variety of operating systems and platforms, such as embedded systems, Windows, macOS, and Linux. When working with hardware that may need to interact with many platforms, such as the DLP LightCrafter, this is crucial.
- UI Capabilities: To design user interfaces that are both visually appealing and responsive, Qt offers a vast number of widgets and tools. This is useful for the project because the DLP projector requires real-time feedback or controls for the DLP projector.
- OpenGL Support: If your application involves any graphical processing or visualization, Qt's support for OpenGL can be beneficial.

4.4.2 User Interface

The user interface plays a significant role in ensuring ease of use for the user and preventing any potential confusion when using the application. This project aimed to incorporate some of the important functions of the projector.

The Figure 4.6a and Figure 4.6b show the UI of the DLP Lightcrafter 9000 GUI version 5.2.0.

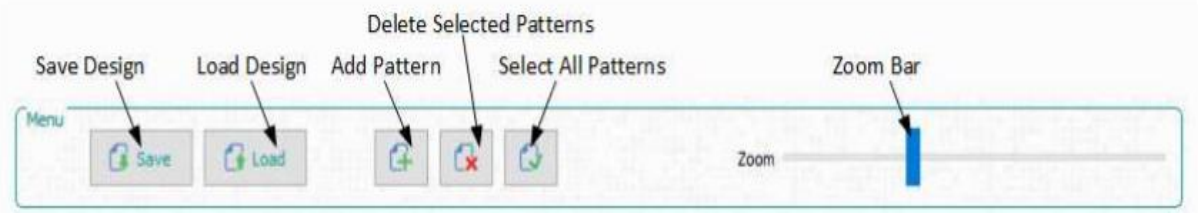

Figure 4.6a Some of the functions of DLP Lightcrafter 9000 GUI version 5.2.0 (Texas Instruments, 2024) [13].

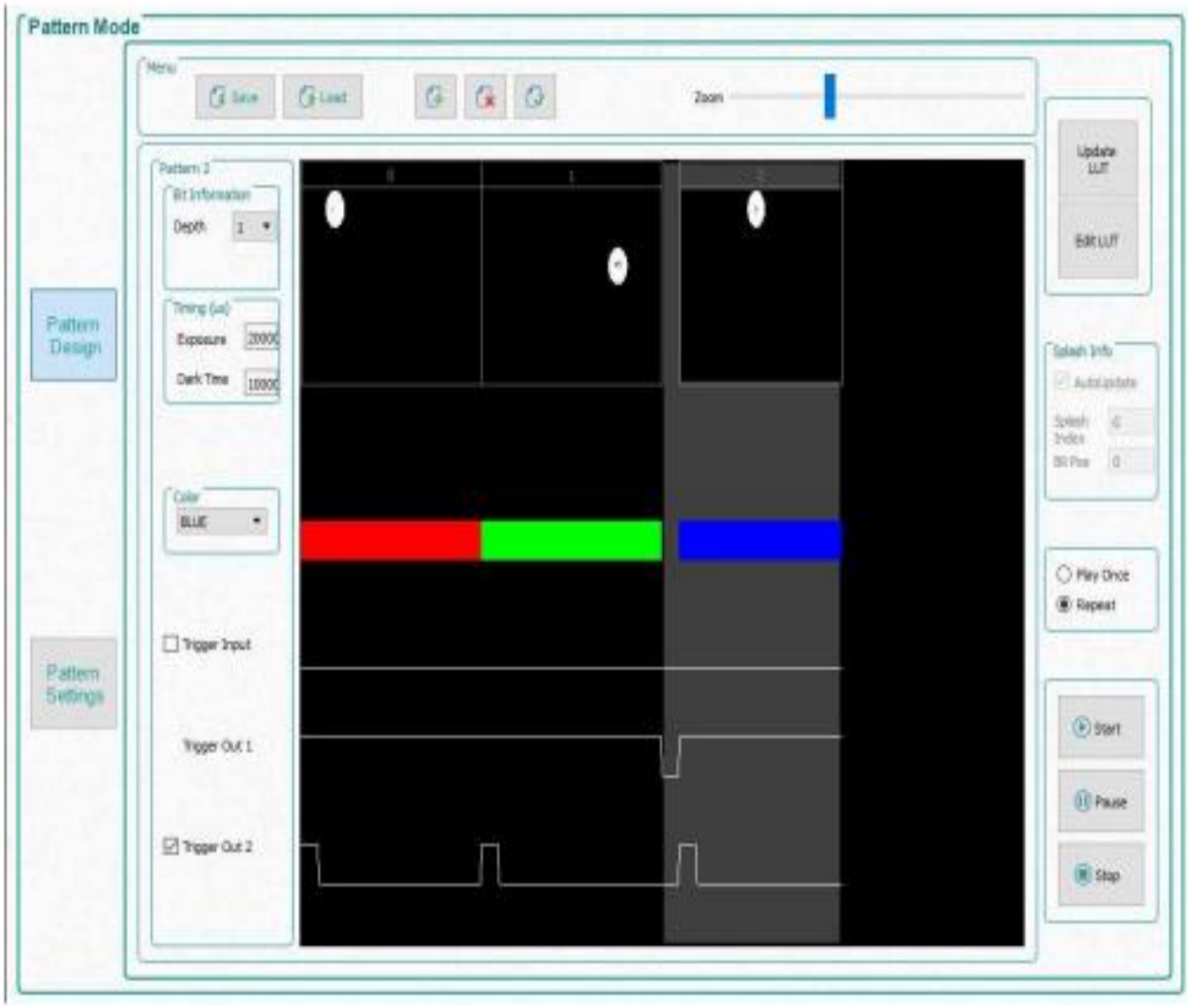

Figure 4.6b Overview of DLP Lightcrafter 9000 GUI version 5.2.0 (Texas Instruments, 2024) [13].

Existing UIs for similar projection systems often exhibit certain limitations. Many of these interfaces may overwhelm users with complex menus and technical jargon, making it difficult for less experienced operators to utilize the software effectively. UI adopted for this project was a more user-friendly application that emphasized clarity and accessibility.

The new interface developed in this project contained only important features that needed to be added and was created and designed to be more simplistic and aimed to lessen the steps required for user to take when using the projector for projection. For future works, important features will be added slowly.

The Figure 4.7 shows the UI of the application developed for this project.

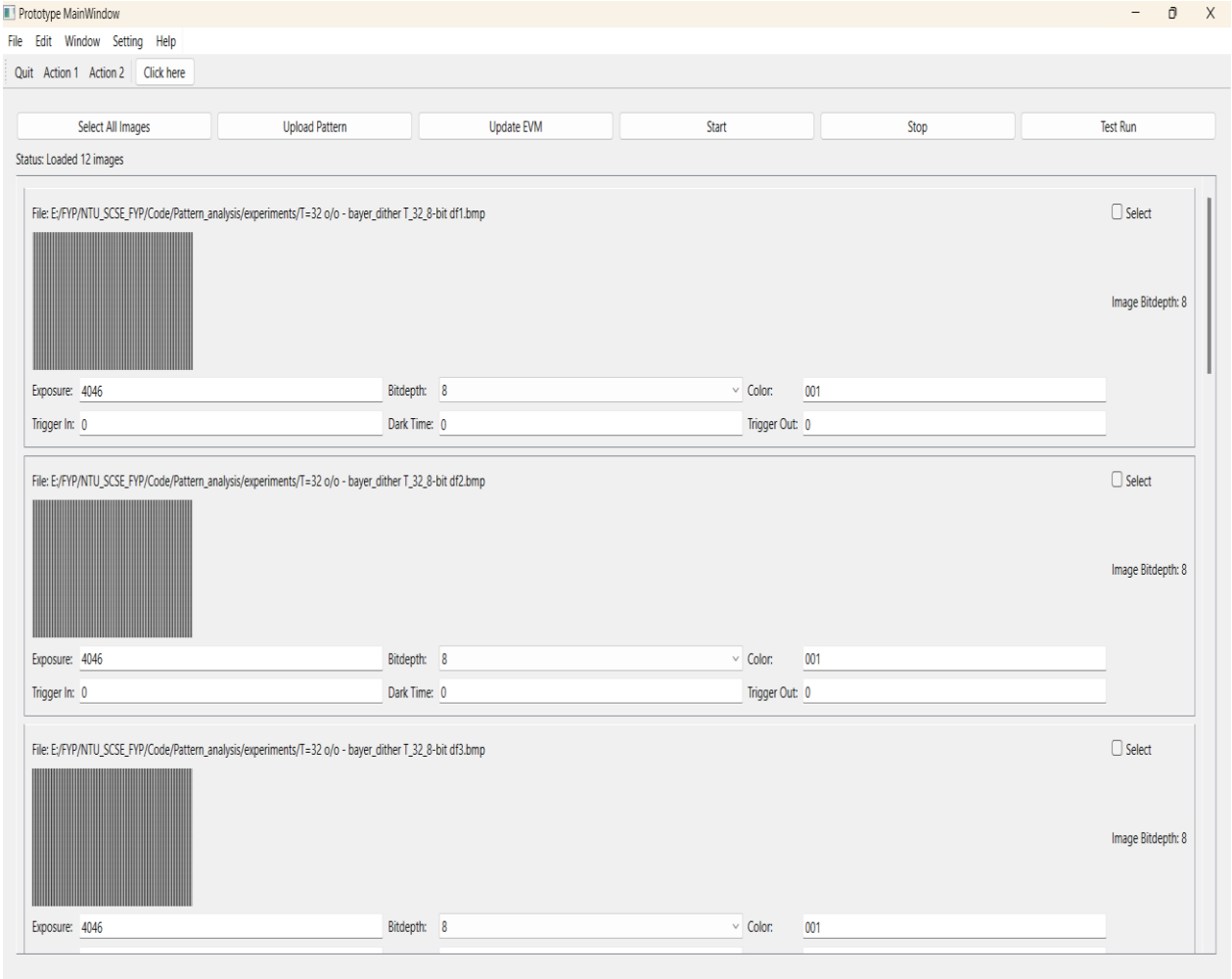

Figure 4.7 User interface developed using Qt Python.

4.4.3 Functionalities

This project incorporated several features available in the original software, alongside custom enhancements designed to improve user experience. The following is a list of the application features, with the corresponding terminology used in the original software indicated in parentheses:

- **Select/Deselect All Images Button** – This function allows users to select or deselect all uploaded images simultaneously.
- **Upload Patterns Button** – This feature facilitates the uploading of patterns to the application (referred to as "Add Patterns" in the original software).

- **Update EVM Button** – This button enables the user to upload modified patterns to the projector (known as "Update LUT" in the original software).
- **Start Button** – This function initiates the projection of the patterns (labelled "Start" in the original software).
- **Stop Button** – This button halts the projection of the patterns (designated as "Stop" in the original software).
- **Display Images** – This function displays each of the patterns uploaded
- **Changing parameters** - This function allows the user to modify exposure time, bit depth, color, dark time, and trigger settings.

These features have been carefully selected and tailored to enhance the application's functionality and usability, ensuring a more efficient workflow for users.

There are also additional functions that make using the application easier to use.

- Selecting certain images by checking them through the checkbox or clicking the “Select All Images” button to select all the images. This action changes the selected image tab to green, providing a visual indication of the user's selections.
- Selected images can then be modified at the same time, for example changing specific images bit depth to other value and exposure times can be modified to the same value at the same time. Shown in the figure below. These functions were extremely useful when dealing with a lot of patterns.

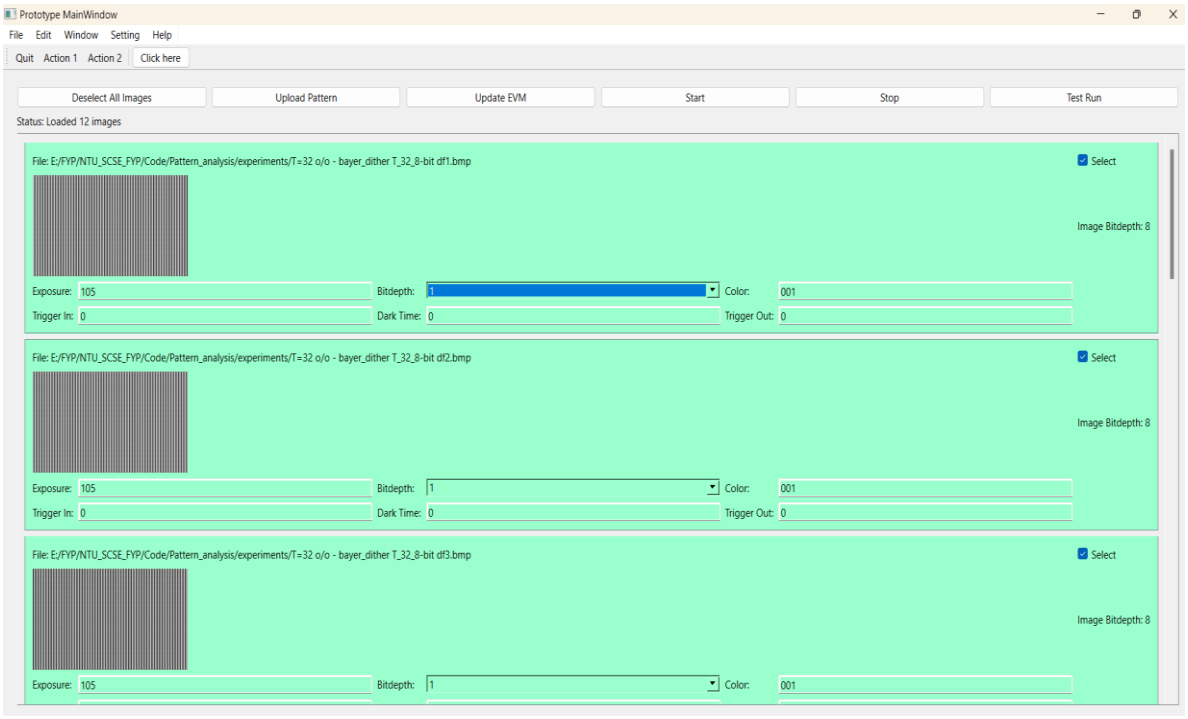

Figure 4.8 "Select/Deselect All Images" Function

The challenge of developing this application was to convert the patterns into data that fit 24-bit that the projector can process. DLP Lightcrafter projector includes the method to convert the patterns into the data to be projected. These data varied for every bit of depth and the different number of patterns.

The application also incorporated backend features, such as reading and processing information from the uploaded patterns. This process involved converting the input pattern bit depth to an 8-bit representation by dividing the image values by a denominator of 2n where n refer to (8 - current bit). The converted information was then used with a data compression technique known as Embedded Run-Length Encoding (ERLE). ERLE reduced the amount of data needed to represent an image while preserving essential information, thereby decreasing the computational resources required.

ERLE operates by encoding sequences of repeated data elements, known as runs, into a compressed format that includes the data value and the number of times it repeats. This approach was particularly effective for compressing data with long sequences of identical values, such as binary images, grayscale images, or other types of uniform data. This method of compression optimized storage and processing efficiency in the application [15].

To manage memory effectively, DLP utilized ERLE to efficiently compress the image data into sets for 24-bit data and transmit the data for high-speed projection. ERLE works by encoding repetitive sequences of pixels in the image, significantly reducing the amount of data required for each frame without compromising visual quality. In a DLP system, where rapid image projection is essential, ERLE helped to minimize the time needed for data transfer and processing, allowing for faster frame rates. This was particularly beneficial in applications like Fringe Projection Profilometry (FPP), where capturing dynamic scenes at high speeds was crucial. By using ERLE, the DLP projector achieves more efficient data handling, enabling smoother operation and higher measurement speeds, making it an effective solution for scenarios requiring real-time high-frequency projection.

The Figure 4.9 shows an example of how ERLE works.

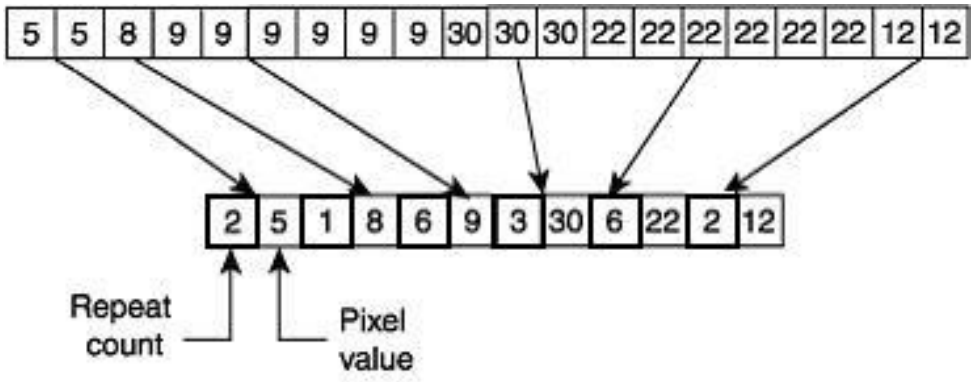

Figure 4.9 ERLE on 8-bit image array [17].

During the encoding phase, each row of the image was processed by identifying patterns and encoding them accordingly. For example, grayscale image row represented by pixel values shown in the figure above, (5,5) was converted to (2,5) where 2 represents the number of repetitions of the pixel and 5 is the pixel value that occurred twice repeatedly.

The encoding format was differentiated between different types of pixel storage whether a run of identical pixels was being recorded or individual pixel values were being stored. After processing all rows, the encoded data was aligned to a 4-byte boundary for optimal storage. For example, an image row containing the sequence [0x0000FF, 0x0000FF, 0x0000FF, 0xFF0000] would be encoded as 0x0000FF 0x0003 (indicating three consecutive blue pixels),

followed by 0xFF0000 (the single red pixel), resulting in a compact representation that minimizes the amount of stored data while preserving the original image information.

For different bits, there was a different number of times data will be loaded to the projector, this was because the maximum load data that can be loaded to the projector is 24-bit data. This meant that for 8-bit images, 3 images can be loaded at once while for 1-bit images, 24 images can be loaded at once. In addition, MBOX_DATA containing exposure time, index, and position of the load will be sent to the projector at the same time as the load data.

Figure 4.10 index and bit position to the projector [14].

This technique was particularly effective for images with large areas of uniform color, significantly reducing the storage requirements compared to traditional pixel-by-pixel encoding.

Other functions related to communication between the projector using Python such as establishing a connection, sending commands, and uploading the patterns to the projector were done with the help of the Python library done by and credited to Pozzi et al. (2017) [18].

Chapter 5

Experiments and Results

This section discussed the experiment and results conducted for this project. The objective of this project was to explore the best effective ways to achieve the best 3D reconstruction by comparing and analysing pattern generation.

The period used for this project experiment was T = 36, This value was assigned consistently throughout the pattern generated in this project and RMS was used to measure how similar the ideal pattern compared to its modified version.

The figure 5.1 shows the patterns after they were defocused and projected by the DLP projector and captured by the camera. An observation can be made that there was a distinction of three dithered projections compared to the projection of the original pattern, while Bayer dither and optimized phase dither projections were closely similar due to the similar starting step of the optimized phase dither technique.

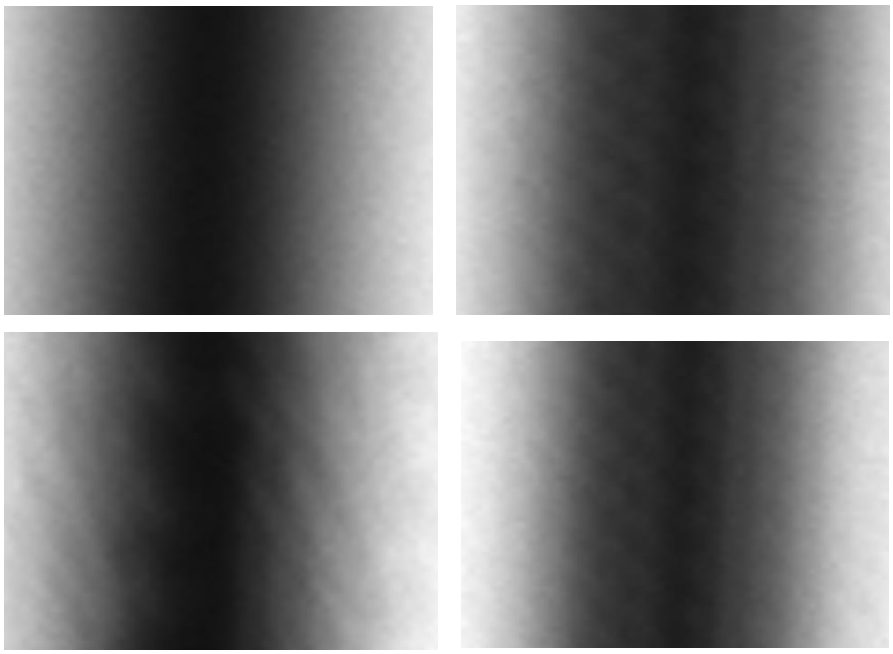

*Figure 5.1 Different pattern representation captured by the camera **(A)** 8-bit fringe pattern, **(B)** Result after Bayer ordered dithering of A, **(C)** Result after error diffusion dithering of A, and **(D)** Result after optimized phase dithering of A.*

For the Bayer Bayer-ordered dithering technique, Bayer matrix size serves as a threshold for the dithering and the challenging part of this dithering technique was to determine the Bayer matrix size to achieve the best results. Root Means Square (RMS) was calculated against different Bayer matrix sizes [2, 4, 8, 16, 32], all these values fit Bayer matrix requirement of 2n size when n is an integer.

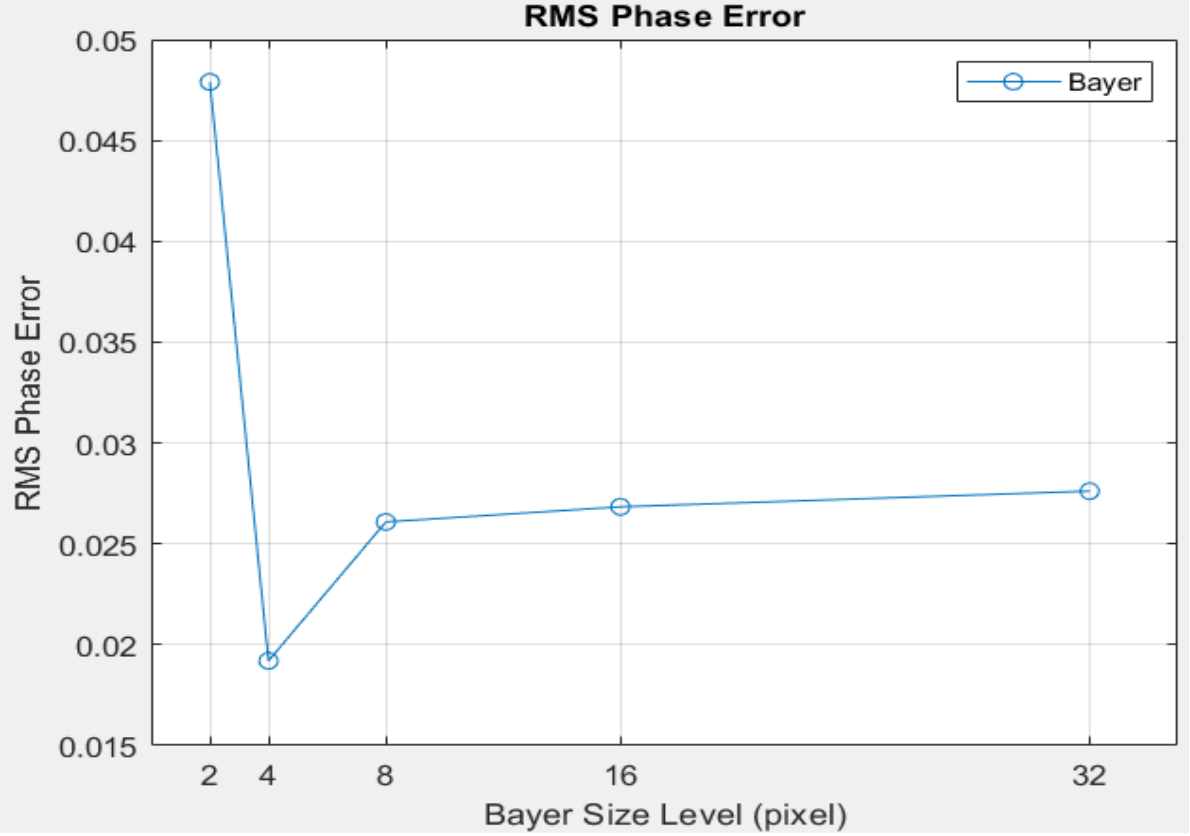

Figure 5.2 RMS error for different Bayer sizes at T = 36.

In Figure 5.2, a 4 x 4 Bayer matrix size yielded the lowest RMS error at approximately **0.019 rad**. Increasing the size of the Bayer matrix did not improve the RMS error score, as the error converged within the range of **0.025 to 0.03 rads**. This indicates that the **4 x 4 matrix** is the optimal size for implementing the Bayer-ordered dithering technique.

The next parameter to be set was the iteration required to perform optimized phase dithering, the challenging aspect of this dithering technique was the significant computational resources required. This was primarily due to the use of a 1080 x 1920 pattern resolution compared to

the 800 x 600 pattern resolution referenced in the paper [8]. One of the steps in optimized phase dithering required pixel mutation / inverted every pixel's value; thus, for a pattern with the resolution of 1080 x 1920 must be processed 2,073,600 times, which was time-consuming and required Heavy-duty computing. To resolve this issue RMS will be measured at every iteration from 0 to 15 to analyze and determine the appropriate maximum of iteration for the algorithm.

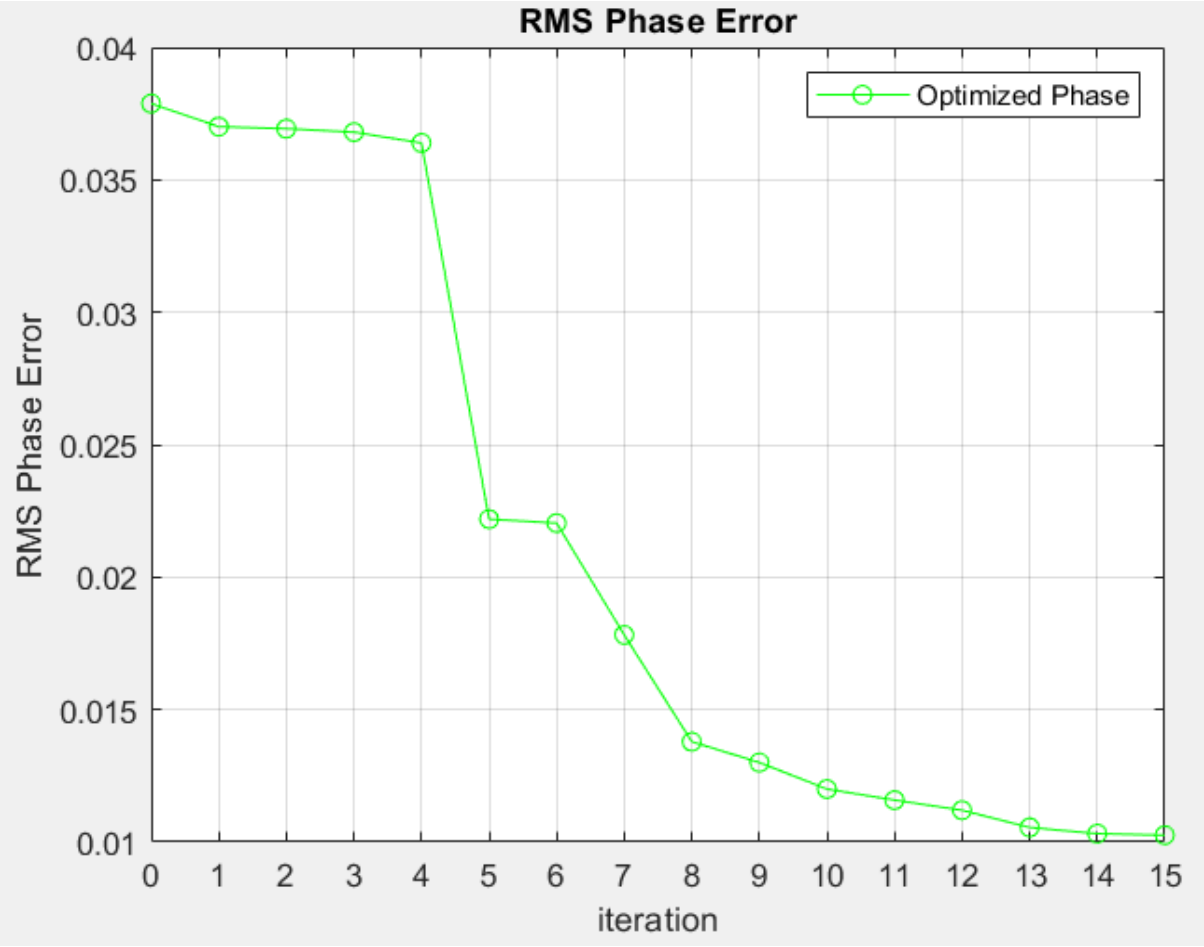

Figure 5.3 RMS error at every iteration for phase optimized dithering at T = 36.

The analysis of the data presented in the Figure 5.3 indicates a significant reduction in the root mean square (RMS) phase error throughout the iterations. Specifically, from the initial iteration to the fifth iteration, the RMS phase error decreased markedly from approximately **0.036392 radians to 0.022188 radians**(difference of 0.0142 radians). Additionally, a further decline in the RMS phase error was observed between the sixth iteration (0.02204 radians) and the eighth iteration (0.013788 radians), which corresponded to a reduction of approximately 0.0083 radians. Subsequent iterations demonstrated increasingly marginal decreases in the RMS phase

error. Subsequent iterations demonstrated increasingly marginal decreases in the RMS phase error, which are small enough to be considered negligible. Based on this analysis, this project has determined that **fifteen iterations** provide an acceptable value for the accuracy of the measurements.

In addition, optimized phase dithering was also implemented with error diffusion dithering at the start instead of Bayer-ordered dithering. However, the RMS error converges at 0.01 after the first iteration of the pixel mutation.

Error diffusion dithering is not suitable for phase-optimized dithering because it processes each pixel in a sequential manner, propagating the quantization error to neighboring pixels. This approach works well for general dithering tasks aimed at creating visually pleasing images but fails to effectively minimize phase errors in phase-optimized applications. The primary issue is that error diffusion relies on a single-pass operation where errors are distributed based on neighboring pixel values, making it difficult to achieve the level of precision needed for accurate phase representation.

In phase-optimized dithering, the goal is to minimize the root mean square (RMS) phase error across the entire pattern, which requires a global optimization approach rather than a local one. Since error diffusion operates iteratively on individual pixels rather than optimizing the pattern holistically, it cannot adequately account for phase continuity and smooth transitions between different regions. Therefore, error diffusion is limited in its capacity to achieve the phase uniformity and low error rates required for high-accuracy applications like Fringe Projection Profilometry (FPP).

The parameter of concern was the amount of defocus to be applied to the dithered pattern. Different numbers of Gaussian filter sizes (defocus level) (1, 3, 5, 7, 9,11, 13) were used and compared with the RMS.

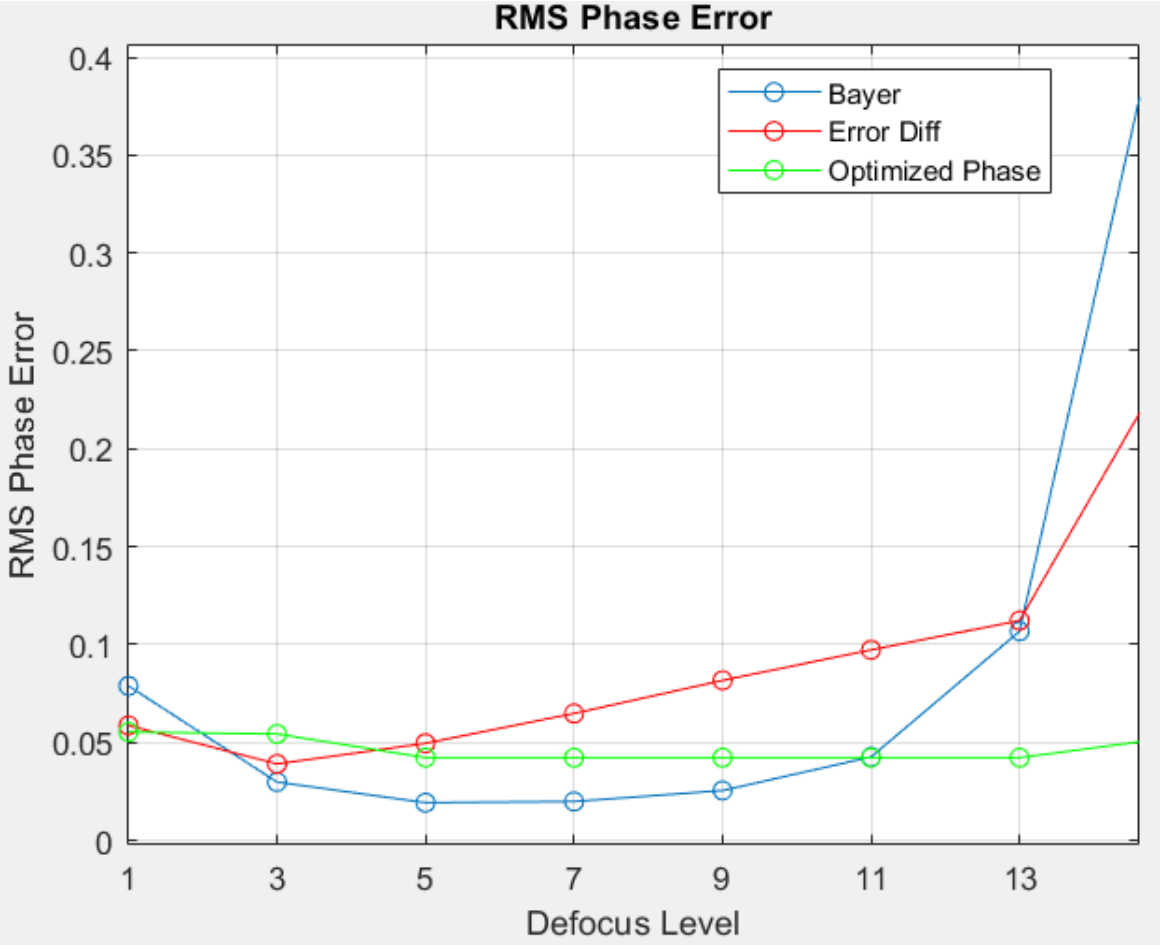

Figure 5.4 RMS error for different defocus level using different dithered pattern at T = 36.

Figure 5.4 illustrates the relationship between defocus levels, represented by the Gaussian filter sizes on the x-axis, and the corresponding RMS phase error. Based on the observations, the most suitable Gaussian filter sizes for minimizing RMS phase error were either 3 (where error diffusion dithering shows the lowest error of **0.0491**) or 5 (where Bayer-ordered dithering shows the lowest error of **0.0495**). The analysis revealed that optimized phase dithering exhibits stable performance across various defocus levels. However, for Bayer-ordered dithering and error diffusion dithering, defocus values beyond 13 resulted in a significant increase in RMS phase error. This project used a **Gaussian filter size of 5** because it provided a balance across all dithering techniques, ensuring consistent results for different methods.

The Figure 5.5 shows the differences between the results of their 2D representation.

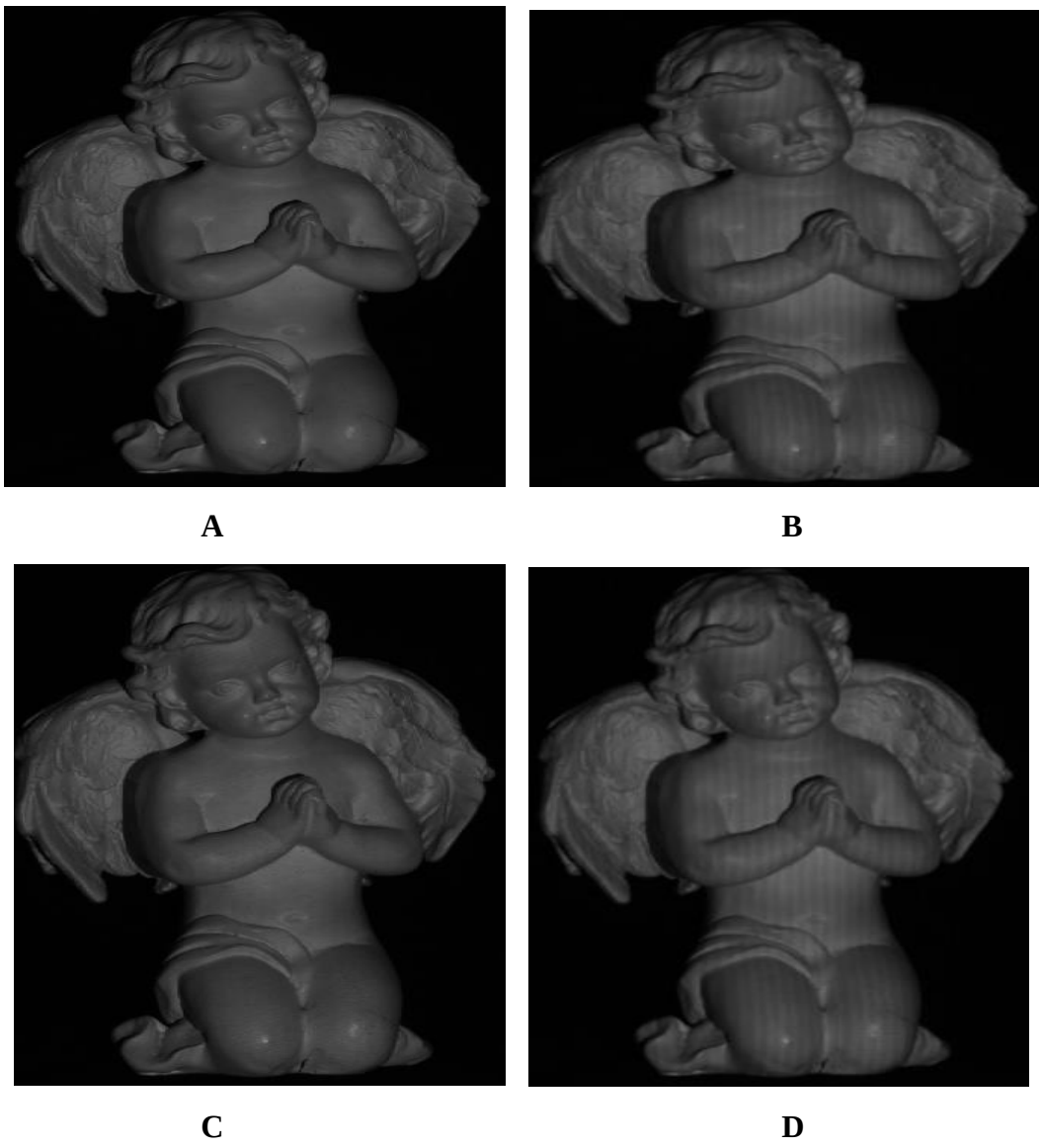

Figure 5.5 2D representation of the 3D reconstruction using: ***(A)*** *original ideal pattern,* ***(B)*** *Bayer ordered dithering,* ***(C)*** *error diffusion dithering, and* ***(D)*** *optimized phase dithering.*

With all the parameter sets, three different sets of three dithered images obtained from dithering the three phase-shifted intensities of ideal patterns were projected on an object. Intensities for ideal patterns were also projected on the same object with the same camera and projector position.

Observation can be made from Figure 5.5 that error diffusion dithering (C) has the closest resemblance to the ideal pattern (A), Both Bayer-ordered dithering and optimized phase dithering were closely resembling the ideal pattern.

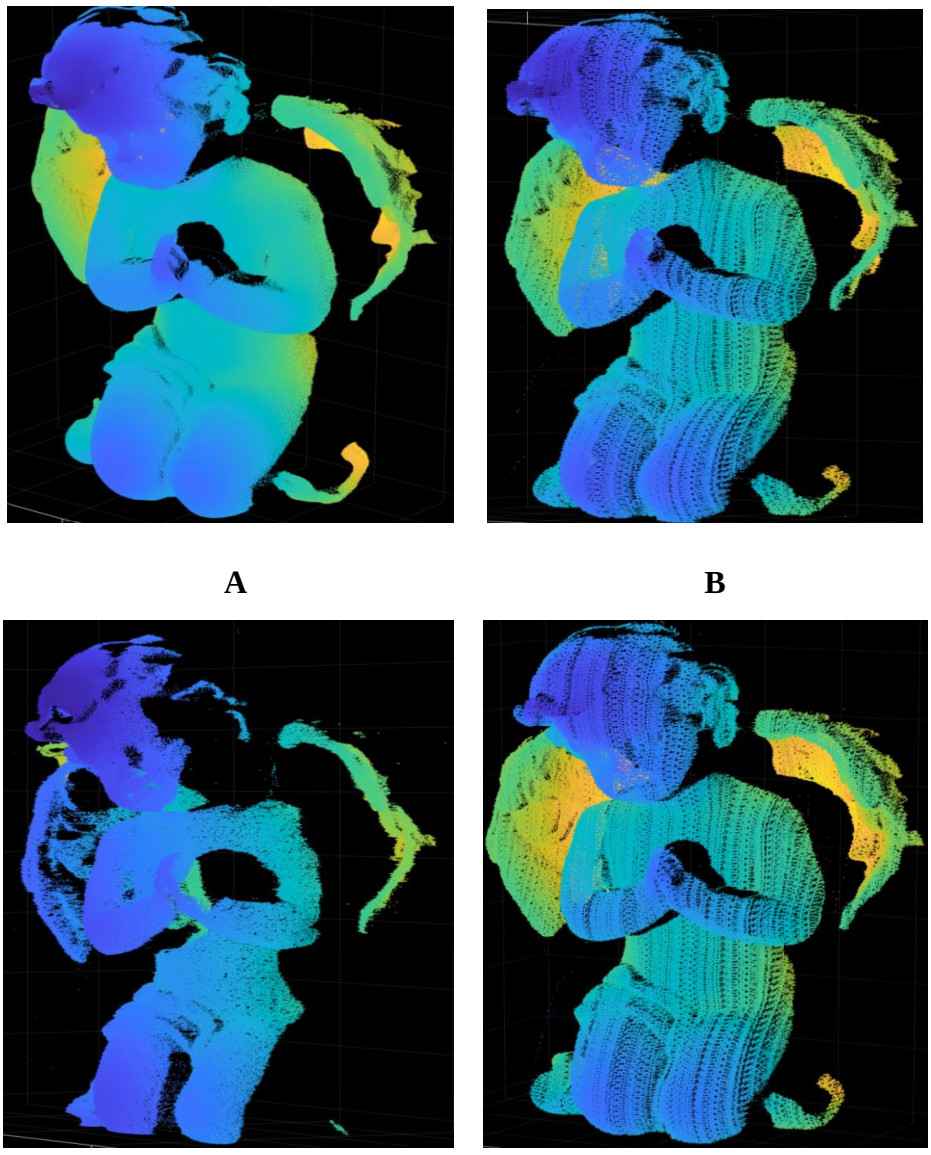

A **B**

C **D**

Figure 5.6 3D representation of the 3D reconstruction using: ***(A)*** *original ideal pattern,* ***(B)*** *Bayer ordered dithering,* ***(C)*** *error diffusion dithering, and* ***(D)*** *optimized phase dithering.*

The Figure 5.6 shows the 3D representation of the results. An observation can be made that the Bayer-ordered dither was like optimized phase dithering, this was due to the optimized phase dithering process including Bayer dither as its first step before performing pixel mutation. Meanwhile, error diffusion consisted of more surface information such as the face and wing details which proved to be better than the other two dithering techniques.

Chapter 6

Conclusion and Future Works

This section provides a comprehensive review of the results achieved in this project, along with potential improvements for future related endeavors. This project explored methods to enhance 3D measurements using Fringe Projection Profilometry (FPP) through optimized pattern projection techniques. Specifically, we implemented a binary defocusing technique to address the speed bottlenecks inherent in DLP projectors, allowing 8-bit patterns to be represented similarly to 1-bit patterns.

Binary defocusing techniques consist of the implementation of binary dithering and projector defocusing. This project explored 3 different techniques of dithering; bayer-ordered dither, error diffusion dither, and optimized phase dither. Through the experiment, we see that error diffusion dithering performed better than bayer-ordered dither and optimized phase dithering.

Lastly, this project developed a standalone application using Qt to edit the patterns uploaded and update them straight to the DLP projector. This application opens the door for adding custom functions required by the user in the future.

Future work could focus on enhancing this application to enable seamless communication between both the camera and the projector. Integrating real-time feedback from the camera would allow for adaptive adjustments to the projected patterns based on environmental conditions or object characteristics, significantly improving measurement accuracy. In addition, the application could also potentially explore advanced algorithms such as pattern recognition and image processing which could help further enhance the system's capabilities, enabling more sophisticated 3D object measurements.

The project demonstrates significant advancements in 3D measurement speed and accuracy, which could potentially impact various applications in different sector, such as industrial inspection, quality control, and biomedical imaging. As we look to the future, further enhancements could include refining the defocusing technique and integrating real-time processing capabilities such as comparing and developing more advanced binary defocusing techniques. This will enable even faster measurement rates and greater precision, paving the way for broader applications in dynamic and complex environments.

References

[1] Zuo, C., Feng, S., Huang, L., Tao, T., Yin, W., & Chen, Q. (2018). Phase shifting algorithms for fringe projection profilometry: A review. *Optics and Lasers in Engineering*, *109*, 23–59. https://doi.org/10.1016/j.optlaseng.2018.04.019

[2] Zhang, H., Vallabh, C. K. P., Xiong, Y., & Zhao, X. (2022). A systematic study and framework of fringe projection profilometry with improved measurement performance for in-situ LPBF process monitoring. Measurement, 191, 110796. https://doi.org/10.1016/j.measurement.2022.110796

[3] Zuo, C., Huang, L., Zhang, M., Chen, Q., & Asundi, A. (2016). Temporal phase unwrapping algorithms for fringe projection profilometry: A comparative review. *Optics and Lasers in Engineering*, *85*, 84–103. https://doi.org/10.1016/j.optlaseng.2016.04.022

[4] Texas Instruments Incorporated. (2014). Interface Protocol. In *DLPU018*.

[5] Lei, S., & Zhang, S. (2009). Flexible 3-D shape measurement using projector defocusing. *Optics Letters*, *34*(20), 3080. https://doi.org/10.1364/ol.34.003080

[6] Li, B., & Zhang, S. (2016). Microscopic structured light 3D profilometry: Binary defocusing technique vs. sinusoidal fringe projection. *Optics and Lasers in Engineering*, *96*, 117–123. https://doi.org/10.1016/j.optlaseng.2016.06.009

[7] Wang, Y., & Zhang, S. (2012b). Three-dimensional shape measurement with binary dithered patterns. *Applied Optics*, *51*(27), 6631. https://doi.org/10.1364/ao.51.006631

[8] Lohry, W., & Zhang, S. (2013). Genetic method to optimize binary dithering technique for high-quality fringe generation. *Optics Letters*, *38*(4), 540. https://doi.org/10.1364/ol.38.000540

[9] Dai, J., & Zhang, S. (2013). Phase-optimized dithering technique for high-quality 3D shape measurement. *Optics and Lasers in Engineering*, *51*(6), 790–795. https://doi.org/10.1016/j.optlaseng.2013.02.003

[10] Lei, S., & Zhang, S. (2010b). Digital sinusoidal fringe pattern generation: Defocusing binary patterns VS focusing sinusoidal patterns. *Optics and Lasers in Engineering*, *48*(5), 561–569. https://doi.org/10.1016/j.optlaseng.2009.12.002

[11] Li, B., Wang, Y., Dai, J., Lohry, W., & Zhang, S. (2013). Some recent advances on superfast 3D shape measurement with digital binary defocusing techniques. Optics and Lasers in Engineering, 54, 236–246. https://doi.org/10.1016/j.optlaseng.2013.07.010

[12] Summerfield, M. (2007). Rapid GUI Programming with Python and Qt (Prentice Hall Open Source Software Development). In Prentice Hall PTR eBooks. https://dl.acm.org/citation.cfm?id=1324804

[13] Texas Instruments Incorporated. (2019). *DLP LightCrafter™ 6500 and 9000 Evaluation Module (EVM) User's Guide*. https://www.ti.com/lit/ug/dlpu028d/dlpu028d.pdf

[14] Texas Instruments. (2024). DLPC900 Programmer's Guide. In *DLPC900 Programmer's Guide* (Manual No. DLPU018J). https://www.ti.com/lit/ug/dlpu018j/dlpu018j.pdf

[15] Stankic, B., Kojic, D., Cvetanovic, M., Dukic, M., Stojanovic, S., & Radivojevic, Z. (2014). ERLE: Embedded run length image encoding. 2014 22nd Telecommunications Forum Telfor (TELFOR), 2, 975–978. https://doi.org/10.1109/telfor.2014.7034569

[16] Chang, C., Lin, C., & Wang, Y. (2006). New image steganographic methods using run-length approach. *Information Sciences*, *176*(22), 3393–3408. https://doi.org/10.1016/j.ins.2006.02.008

[17] *Compression - TRCCompSci - AQA Computer Science*. (n.d.). http://trccompsci.online/mediawiki/index.php/Compression

[18] Pozzi, P., Wilding, D., Soloviev, O., Verstraete, H., Bliek, L., Vdovin, G., & Verhaegen, M. (2017c). High speed wavefront sensorless aberration correction in digital micromirror based confocal microscopy. Optics Express, 25(2), 949. https://doi.org/10.1364/oe.25.000949